Thermodynamic structure of collision-dominated expanding plasma: Heating of interplanetary coronal mass ejections

Y. Liu, J. D. Richardson, J. W. Belcher, and J. C. Kasper

Kavli Institute for Astrophysics and Space Research, Massachusetts Institute of Technology, Cambridge, Massachusetts, USA

H. A. Elliott

Space Science and Engineering, Southwest Research Institute, San Antonio, Texas, USA

[1]   We investigate the thermodynamic structure of interplanetary coronal mass ejections (ICMEs) using combined surveys of the ejecta between 0.3 and 20 AU. ICMEs are shown to have a moderate expansion in the solar wind compared with theoretical predictions. The expansion seems to be governed by a polytrope with $\gamma \sim 1.3$ in this distance range. We find that Coulomb collisions are important contributors to the ion-ion equilibration process in the ICME plasma. The alpha-proton differential speed quickly drops to below 10 km s^{-1} due to strong Coulomb collisions. However, the two species of particles are far from thermal equilibrium with a temperature ratio $T_\alpha/T_p = 4-6$, suggestive of a preferential heating of alpha particles. The plasma heating rate as a function of heliocentric distance required for the temperature profile is deduced by taking into account the expansion and energy transfer between protons and alphas via Coulomb collisions. The turbulence dissipation rate is also inferred from the inertial range power spectrum of magnetic fluctuations within ICMEs. Comparison of the turbulence dissipation rate with the required heating rate shows that turbulence dissipation seems sufficient to explain the ICME heating. Sources powering the turbulence are also investigated by examining the instabilities induced by temperature anisotropies and energy deposition by pickup ions.

1. Introduction

[2]   Coronal mass ejections (CMEs) are large-scale magnetic structures expelled from the Sun due to explosive processes in the solar atmosphere. The ejected material in the solar wind, a key link between activities at the Sun and disturbances in the heliosphere, are now referred to as interplanetary coronal mass ejections (ICMEs). ICMEs are generally described as flux ropes which remain magnetically connected to the Sun as they propagate in the solar wind [e.g., *Burlaga*, 1988; *Bothmer and Schwenn*, 1998].

[3]   ICMEs have been investigated using in situ measurements from spacecraft for over 3 decades. Plasma and magnetic field signatures of ICMEs in these measurements include depressed proton temperatures, enhanced helium abundance, bidirectional streaming of electron strahls, declining velocity profiles, charge state and compositional anomalies, and smooth magnetic fields [*Neugebauer and Goldstein*, 1997, and references therein]. The low temperature, which is generally present within ICMEs [*Richardson and Cane*, 1993], makes the ICME plasma collision-dominated as the plasma expansion time is close to or even larger than the Coulomb collision time (see Appendix A). The importance of the strongly collisional nature of the ICME plasma in regulating ion properties will be studied in this work. ICMEs often undergo expansion in the solar wind since their leading edges usually move faster than the trailing edges and/or their internal pressures are higher than in the ambient solar wind. As a result, the ICME plasma is expected to expand and be collision-dominated, which has significant consequences for modeling the realistic thermodynamics of ICMEs.

[4]   Recent global MHD modeling of ICMEs [e.g., *Odstrcil et al.*, 2002; *Riley et al.*, 2003; *Manchester et al.*, 2004] provides a useful tool for interpreting the observations. In these simulations a polytropic gas with index $\gamma < 5/3$ is assumed to keep the physics of energy
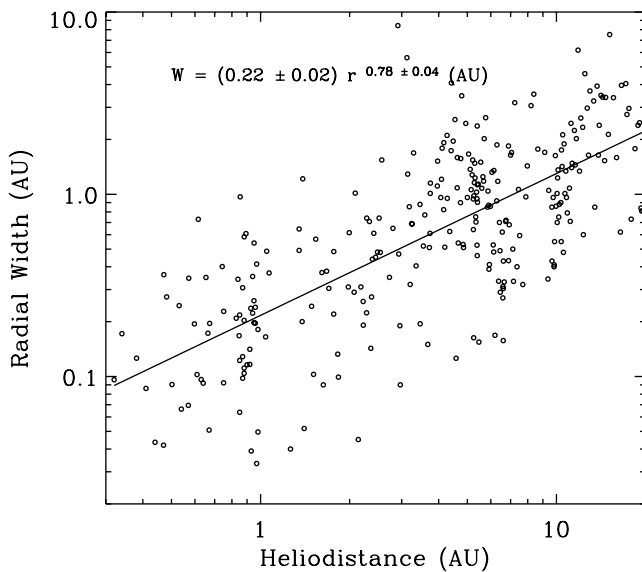
Figure 1. Radial widths of interplanetary coronal mass ejections (ICMEs) as a function of heliocentric distance. The solid line shows the best power law fit to the data. The fit result is given by the text in this figure.

transport simple while retaining a fair amount of plasma heating. The polytropic process, in theory, is entropy-conserving and thus reversible, whereas the actual heating may be irreversible. *Leamon et al.* [1998b] examined the properties of magnetic fluctuations within an ICME at 1 AU and found that the power spectrum of the fluctuations shows a steepening at high frequencies, indicative of the onset of magnetic dissipation. Dissipation of turbulence has been considered the mechanism responsible for the solar wind heating in the past decade [e.g., *Goldstein et al.*, 1995; *Matthaeus et al.*, 1999; *Smith et al.*, 2001]. The magnetic fluctuations represent nonlinear interacting modes of the system. The nonlinear interactions produce a flow of energy originating from low frequencies (large scales), which cascades through the inertial range (typically with a $f^{-5/3}$ form) and is then converted to thermal energy in the dissipation range (small scales). This spectral transfer can lead to significant heating of the plasma and is inherently irreversible. This intrinsic difference between the polytropic process and turbulence dissipation makes the modeling of the thermodynamic state of ICMEs a challenge. There is a large gap in our understanding of the microphysics governing the energy transport process and the ICME signatures.

[5] Observations of ICMEs over a range of radial distances in the heliosphere can constrain models of their thermodynamic structure. Recently, *Liu et al.* [2005] performed a statistical study of ICMEs from 0.3 to 5.4 AU using a multispacecraft survey. *Wang and Richardson* [2004] extended this research out to 30 AU based on the observations of Voyager 2. Combining these surveys with theoretical analysis, this paper investigates the thermody-namic state of ICMEs. In the next section, we demonstrate that ICMEs expand and Coulomb collisions are important within ICMEs. Section 3 contains theoretical analysis of the heating problem along with a discussion of the source of the turbulence. We close by summarizing our results in

section 4 and provide an appendix describing the derivation of formulations used in the analysis.

2. Observations and Data Analysis

[6] Two difficulties have stymied the development of a comprehensive view of ICMEs individually and as a class. The first is how to best identify ICMEs in the solar wind. Despite the plethora of ICME signatures, the identification of ICMEs still remains subjective. No individual character-istic is necessary and sufficient to define the presence of an ICME. Second, spacecraft are usually sparsely distributed and rarely radially aligned. Tracking specific ICMEs through the heliosphere is thus generally not possible.

[7] A statistical representation of ICME properties bypasses the second difficulty, although the first one still applies. In this work, we combine different surveys of ICMEs to study their radial evolution. The first survey was conducted by *Liu et al.* [2005] from the Helios 1 and 2, Wind, Ace, and Ulysses data. These spacecraft are at helio-spheric distances ranging from 0.3 to 5.4 AU. The criteria used to select ICMEs were that the observed proton temper-ature, T_p, is less than 0.5 of the expected temperature, T_{ex}, and the density ratio of alpha particles to protons, n_α/n_p, is larger than 8%. The expected temperature, essentially the typical temperature for normal solar wind, is inferred from the well-established relationship between the solar wind temperature and speed [e.g., *Lopez*, 1987]. By including the radial temperature gradient, this relationship can be applied at different radial distances. *Wang and Richardson* [2004] used the temperature criteria to identify ICMEs from Voyager 2 data out to 30 AU. Both of these surveys incorporated other signatures to determine the ICME boundaries. In order to make the statistical average more reliable, we searched the Voyager 1 data for more events employing the same method as Wang and Richardson. We cut off the study at 20 AU since the temperature criteria may become less reliable due to the heating of pickup ions. Furthermore, we use only the data within ±20° in latitude to assure a meaningful comparison of different data sets.

2.1. Expansion of ICMEs

[8] Under these constraints, the above surveys yield about 280 ICMEs at Helios 1 and 2, Ulysses, Voyager 1 and 2. Figure 1 shows the radial widths of ICMEs versus distance from 0.3 to 20 AU. The radial width is the time duration of the ICME multiplied by the average speed. The best power law fit, obtained with least squares analysis, is represented by the solid line. The radial width increases with distance, with average values of about 0.22 AU at 1 AU and about 1.33 AU at 10 AU. A large scatter is seen in the outer heliosphere. *Wang and Richardson* [2004] showed that about 40% of the solar wind is ICME material at 15– 20 AU near solar maximum.

[9] Two factors may contribute to the expansion of ICMEs. First, the magnetic field inside most ICMEs in the inner heliosphere is larger than in the ambient solar wind (see Figure 2). The higher magnetic field, which dominates the internal pressure of ICMEs, may cause the ICME plasma to expand. The magnetic pressure, however, may be balanced by the magnetic tension for a force-free
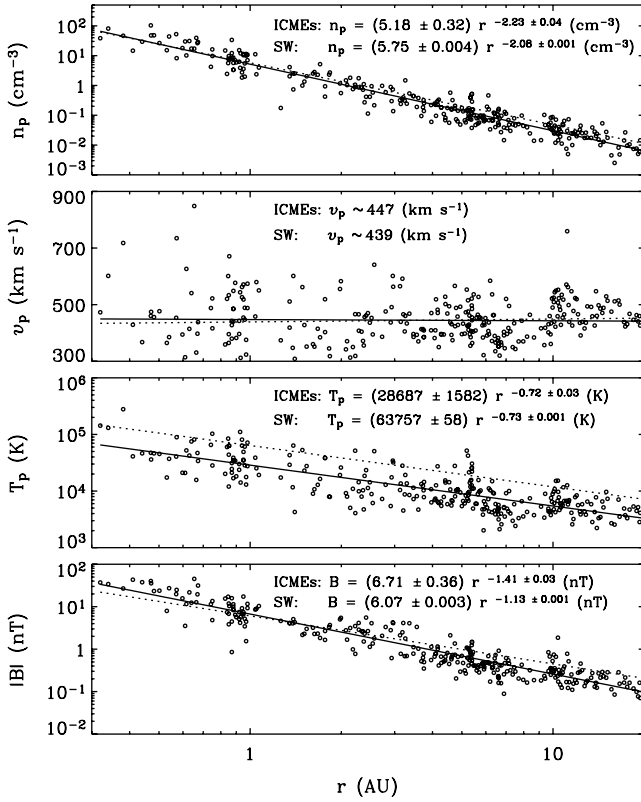
Figure 2. The average proton density, speed, temperature, and the magnetic field strength in each ICME. Also displayed are fits to the ICME data (solid lines) and fits to the ambient solar wind (dotted lines), together with corresponding fit parameters (text).

CMEs in the solar atmosphere. In the outer heliosphere (5–10 AU), ICMEs are frequently seen as low-pressure regions accompanied by declining speed profiles. This characteristic provides evidence for the overexpansion of ICMEs but may also indicate the effect of the speed difference on the expansion. The contribution from the speed difference may be dominant in MC expansion with a small magnetic force involved.

[10] The expansion of ICMEs can also be inferred from the plasma observations. Figure 2 displays the radial variation of the proton density n_p, bulk speed v_p, proton temperature T_p, and the magnetic field magnitude B. The solid and dotted lines show the best power law fits to the ICME and solar wind data, respectively. Fit results are given by the text in each panel. The top and bottom panels indicate that the density and magnetic field within ICMEs decrease faster with distance than in the ambient solar wind, as expected if the ICMEs expand. ICMEs have a larger magnetic field than the ambient solar wind within 1 AU, which may contribute to the expansion of ICMEs as discussed above. The second panel suggests that the average ICME speed is comparable to the solar wind speed and remains constant in this distance range. The third panel shows that lower temperatures are seen within ICMEs than
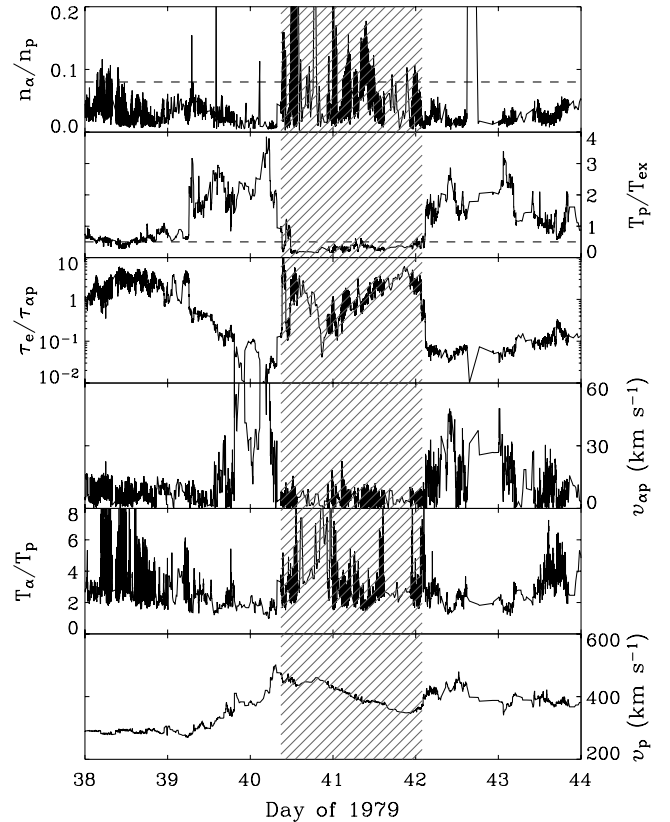
configuration of the field [e.g., *Suess*, 1988; *Cargill et al.*, 1997]. A magnetic field **B** is said to be force-free if the current density, **j**, is aligned with the field. Magnetic clouds (MCs), a subset of ICMEs with smooth rotation of the magnetic field, have often been characterized by such a topology. In general, **j** and **B** are not exactly parallel due to the existence of a finite thermal pressure, p. The angle χ between the current density and the magnetic field can be estimated from $\sin \chi = \frac{|\mathbf{j} \times \mathbf{B}|}{jB}$. Consider MHD equilibrium, i.e., $\mathbf{j} \times \mathbf{B} - \nabla p = 0$. It can be readily shown that

$$\sin \chi \simeq \frac{p}{B^2/\mu_0} = \frac{1}{2}\beta,$$

where μ_0 is the permeability of free space. Here we assume that the length scales for the spatial variations of the magnetic field and gas pressure are of the same order in magnitude. The observed proton beta is usually $0.1-0.2$ and the electron temperature is ~ 3 times the proton temperature in ICMEs [*Liu et al.*, 2005]. Therefore the total plasma beta is $0.4-0.8$, which gives an angle $\chi = 12-24°$ from the above equation. Considerable departures from force-free equilibrium exist for common ICMEs, so the overpressure may result in the ICME expansion. Second, the leading edges of ICMEs usually move faster than the trailing edges. The speed difference may result from the overpressure within ICMEs or may be a residual effect of the initiation of

Figure 3. An ICME (hatched area) observed by Helios 1 at 0.98 AU. From top to bottom the panels show the alpha-to-proton density ratio, the observed-to-expected temperature ratio of protons, the expansion time over the Coulomb collision time, the differential speed between alphas and protons, the alpha-to-proton temperature ratio, and the bulk speed of protons. The dashed lines in the upper two panels mark the limits of the identification criteria.
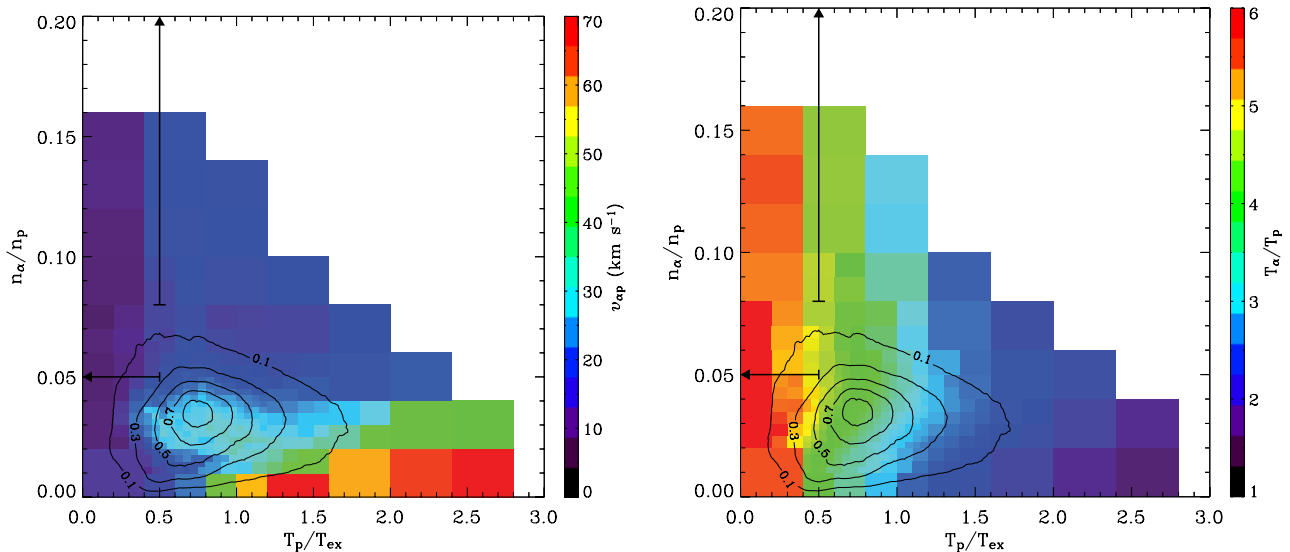
Figure 4. Surveys of the differential streaming $v_{\alpha p}$ (left panel) and the temperature ratio T_α/T_p (right panel) between alphas and protons, as a function of the density ratio n_α/n_p and the normalized temperature T_p/T_{ex}. The whole Helios 1 data set is used and divided into cells in the plane; regions with dense measurements contain more cells while no cell has less than 1000 spectra. The color scales indicate the average values within the bins. Black contours show the two-dimensional histogram of the data. The regions with $n_\alpha/n_p \geq 8\%$ or $T_p/T_{ex} \leq 0.5$ are shown by the arrows.

in the solar wind, as required by the ICME selection criteria. The expansion of ICMEs might be expected to result in a faster temperature decrease in ICMEs than that of the background solar wind due to adiabatic cooling. However, the temperature has a similar slope for ICMEs and the solar wind. Suppose that the ICME plasma can be described by a polytrope. The polytropic index, derived from the relation $T_p n_p^{1-\gamma} = $ const, is ~1.3 based on the fits in Figure 2, which is less than the adiabatic value 5/3. The physical interpretation is that local heating of the plasma must occur as ICMEs expand and move outward. We will investigate the heating mechanism in the next section.

2.2. Coulomb Collisions and Ion Properties

[11] Understanding the thermodynamic state of ICMEs requires knowledge of the kinematic properties of the different ions in the ICME plasma and how they differ from those in the solar wind. Extensive studies of the solar wind show that heavy ions usually move faster than protons with the relative motion along the local magnetic field and are significantly hotter than protons [e.g., *Feldman et al.*, 1974; *Neugebauer*, 1976; *Marsch et al.*, 1982; *Neugebauer et al.*, 1996; *Reisenfeld et al.*, 2001]. Since the ICME plasma has a much lower temperature, ion properties in ICMEs may be different from those in the solar wind. An important consequence of the low temperature is that the Coulomb collision time between different particles, proportional to $T^{1.5}/n$ (see equations (A4) and (A5)), may be small compared to the expansion time of the plasma. Coulomb collisions should thus play an important role in the ion-ion equilibration process in the ICME plasma.

[12] A typical example of an ICME is displayed in Figure 3 (hatched area). This event was observed by Helios 1 at 0.98 AU. Enhanced helium abundance (top panel) and depressed proton temperature (second panel)

were used to identify this event. The third panel shows the expansion time τ_e divided by the Coulomb collision time $\tau_{\alpha p}$ (see Appendix A). This ratio, typically larger than unity within this event, is greatly boosted by the low temperature but drops to the order of 10^{-1} in the ambient solar wind. Particles in the ICME plasma therefore have plenty of time for collisions. Owing to the strong Coulomb collisions the differential speed between alphas and protons, $v_{\alpha p} = |\mathbf{v}_\alpha - \mathbf{v}_p|$, is very small, which can be clearly seen in the fourth panel. The temperature ratio, T_α/T_p, is shown in the fifth panel. The short collision time suggests that the ions should be in thermal equilibrium. Surprisingly, T_α/T_p is higher within the ICME than in the ambient solar wind. The alpha particles must be preferentially heated; the preferential heating is not balanced by the energy loss to protons via Coulomb collisions. The above situation also occurred on days 38–39 when the temperature was reduced together with a small increase in the helium density. Also shown in this figure is the velocity of protons (bottom panel), which decreases across the ICME, suggestive of expansion of the event.

[13] A global view of the differential speed and temperature ratios between alphas and protons in different plasmas is shown in Figure 4, based on 40 s averages of Helios 1 measurements. The whole data set, containing about 800,000 spectra, is binned into cells in the $(n_\alpha/n_p, T_p/T_{ex})$ plane; wherever the data density permits, the bins are further subdivided, but each bin contains at least 1000 data points. The color bars indicate the average values in each bin for the two parameters. The black contours show the relative density of the measurements at the levels of 0.1, 0.3, 0.5, 0.7, and 0.9. The most probable state of the solar wind between 0.3 and 1 AU has $v_{\alpha p} \sim 30$ km s^{-1} and $T_\alpha/T_p \sim 3$– 4, but note that radial variations may be present in the two quantities. Comparing the two panels, we find that the
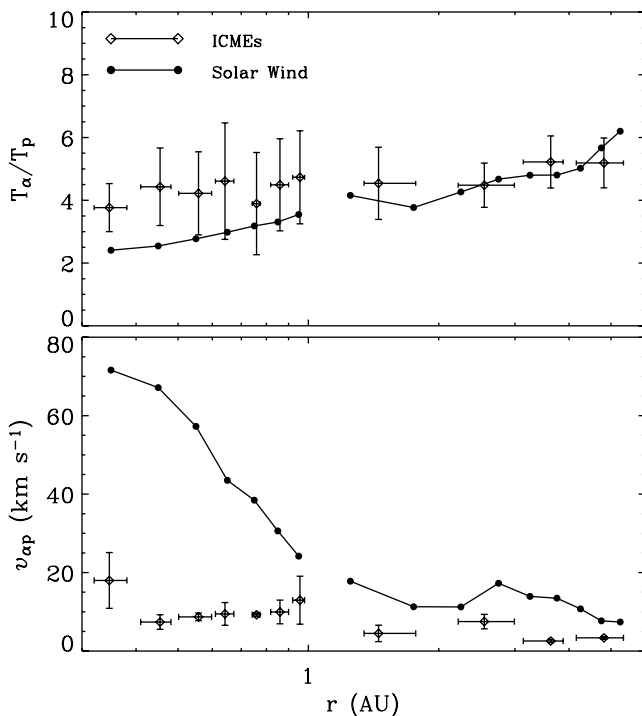
Figure 5. Radial variations of T_α/T_p (upper panel) and $v_{\alpha p}$ (lower panel) for ICMEs (diamonds) and solar wind (filled circles). For ICMEs, the horizontal bars indicate the bounds of the bins, while the error bars show the standard deviation of the parameters within the bins. The solar wind levels are represented by the average values over 0.1 AU bins within 1 AU and 0.5 AU bins beyond. All the data are within ±20° in latitude.

differential speed $v_{\alpha p}$ and the temperature ratio T_α/T_p are anticorrelated. The regions with high helium density and/or low proton temperature can be classified as the ICME plasma. In these regions the differential streaming is reduced by strong Coulomb collisions to below 10 km s^{-1}, whereas the alpha-to-proton temperature ratio is about 5 or even higher. This picture is in agreement with the scenario for the individual case discussed above. Another interesting area is the lower right corner of the panels with low helium density and high proton temperature. The extremely high temperature suggests that Coulomb collisions are of negligible importance for energy transfer between particles. In support of this point, the speed difference reaches 60–70 km s^{-1}, the highest value shown by the left color bar. However, the temperature ratio of alphas to protons is only 1–2 in this area, the lowest level indicated by the right color bar.

[14] The radial evolution of T_α/T_p and $v_{\alpha p}$ from 0.3 to 5.4 AU is shown in Figure 5, with diamonds and dots corresponding to ICMEs and solar wind, respectively. Only the Helios and Ulysses data are shown as measurements for alpha particles are not routinely available from the Voyager missions. The Ulysses ion spectrometer has an angular resolution of 5° in the polar direction, so the perpendicular velocity has large uncertainties. To overcome this difficulty, we follow the approach of *Reisenfeld et al.* [2001] and calculate the differential speed as $v_{\alpha p} = $

$\left|\frac{v_\alpha - v_p}{\cos\theta_B}\right|$, using the fact that the relative streaming is along the magnetic field [e.g., *Marsch et al.*, 1982]. The variables v_α and v_p are the velocities of the alpha particles and protons, respectively, and θ_B is the angle between the magnetic field vector and the radial direction. Only the data with $|\cos\theta_B| \geq 0.3$ is included to guarantee a reliable differential speed. For an individual ICME, this procedure eliminates many data points; we use only the cases where over 60% of the points remain. Since Helios observations are at low latitudes, we use only Ulysses data within ±20° of the ecliptic plane. The solar wind data with ICMEs removed is binned over 0.1 AU intervals inside 1 AU and over 0.5 AU intervals beyond 1 AU. Binning is also performed for ICMEs, with the bin size indicated by the horizontal bars; the bounds of each bin are chosen to ensure enough points for the average. The standard deviation for each ICME bin is represented by the error bars. Radial dependences of solar wind parameters have previously been compiled [e.g., *Marsch et al.*, 1982; *Neugebauer et al.*, 1996; *Reisenfeld et al.*, 2001]. Note that here we only include the low-latitude data and do not differentiate between fast and slow streams.

[15] The differential streaming in the solar wind (lower panel) shows a fairly steady decrease with distance, probably due to the accumulative effect of Coulomb collisions, in agreement with *Marsch et al.* [1982] and *Neugebauer et al.* [1996]. In contrast to the solar wind, the ICME $v_{\alpha p}$ decreases to less than 10 km s^{-1} by 0.4 AU. The temperature ratio T_α/T_p does not vary with distance in ICMEs but does in the solar wind. Evidently, this ratio is larger than that of the solar wind inside 1 AU but roughly the same magnitude beyond 1 AU. The invariance of the ICME temperature ratio with distance implies the existence of a local mechanism responsible for heating the alphas. One may consider that the free energy associated with the differential streaming is converted into the thermal energy of the plasma. *Reisenfeld et al.* [2001] found a rough balance between the free energy and the required heat input for the alpha particles in the high-latitude solar wind. It is not likely that the free energy preferentially goes to alphas through Coulomb collisions. In addition, the differential speed within ICMEs is very small outside about 0.4 AU, but the temperature ratio is conserved at much larger distances. We conclude that the differential streaming, a relic in the initial helium acceleration in the solar atmosphere, does not account for the observed ICME heating.

3. Heating Mechanism and Energy Budget

[16] The expansion of ICMEs is governed by a polytrope of $\gamma \sim 1.3$. This result implies thermal input into the ICME plasma. *Kumar and Rust* [1996] proposed a current-core flux-rope model for MCs in which the energetics of the expansion are controlled by the magnetic helicity conservation. Their theoretical calculation shows that at least 58% of the magnetic energy lost in the expansion is available for the heating. Thus they suggested that the heating may result from the local magnetic dissipation. In the case of the solar wind, this dissipation usually appears as a spectral break in the power spectrum of magnetic fluctuations in association with the proton gyrofrequency [e.g., *Goldstein et al.*, 1995, and references therein].
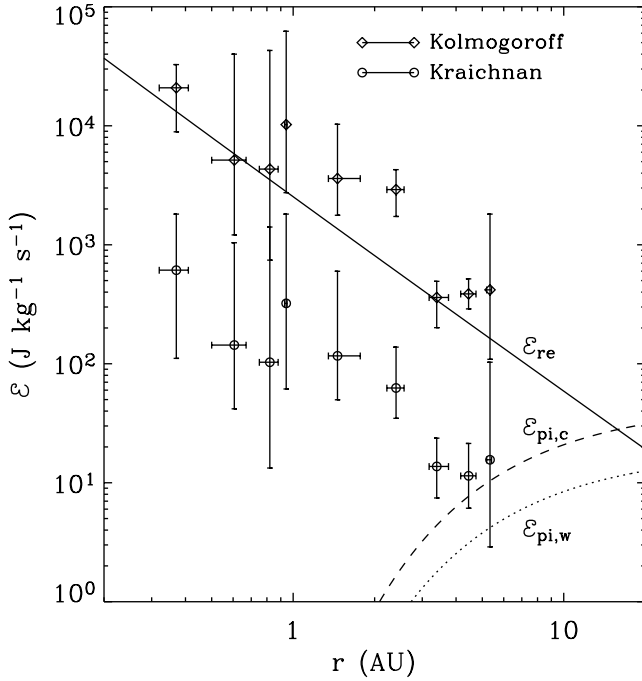
Figure 6. Energy dissipation rate of magnetic fluctuations within ICMEs deduced from Kolmogoroff's law (diamonds) and from Kraichnan's formulation (circles), respectively. Binning is similar to Figure 5; the error bars indicate the lower and upper bounds of the data for each bin. Also plotted are the required heating rate (solid line) determined from equation (2) and the energy deposition rate by pickup ions inferred from the collision approach (dashed line) and from wave excitation (dotted line).

Similar results were also obtained in a case study of ICMEs, but the spectrum shows less steepening in the dissipation range compared with that of the solar wind [*Leamon et al.*, 1998b]. Magnetic dissipation is considered by the turbulence interpretation to be the ultimate fate of the low-frequency magnetic power residing at large scales. In this section, we will examine the role of magnetic turbulence in the heating of ICMEs.

3.1. Required Heating Rate

[17] In Appendix A, we derive the equations of temperature evolution for protons and alphas, taking into account the Coulomb energy transfer between them. Knowing the properties of the ICME expansion, we can use these equations to determine the heating rate required to produce the observed temperature profile. Inversion of equations (A12) and (A14) results in the specific heating rates of protons and alphas expressed as

$$\varepsilon_p = \frac{k_B T_p}{m_p}\left[\frac{3v}{2}\frac{d}{dr}\ln T_p - \frac{3\left(\frac{T_\alpha}{T_p}-1\right)}{2\tau_{p\alpha}} + \frac{1}{\tau_e}\right],$$

$$\varepsilon_\alpha = \frac{k_B T_\alpha}{m_\alpha}\left[\frac{3v}{2}\frac{d}{dr}\ln T_\alpha - \frac{3\left(\frac{T_p}{T_\alpha}-1\right)}{2\tau_{\alpha p}} + \frac{1}{\tau_e}\right]. \quad (1)$$

The total required heating rate is then simply

$$\varepsilon_{re} = \varepsilon_p + \varepsilon_\alpha. \quad (2)$$

On the basis of the power-law fits to the data in Figure 2, we can quantitatively evaluate the required heating rate as a function of heliocentric distance. We assume fixed density and temperature ratios for protons and alphas within ICMEs, i.e., $\frac{n_\alpha}{n_p} \simeq 0.08$ and $\frac{T_\alpha}{T_p} \simeq 4.5$ (see Figure 5). Note that the density profile, which helps determine the timescales of τ_e, $\tau_{\alpha p}$, and $\tau_{p\alpha}$, is also needed in the calculation. The resulting heating rate is displayed in Figure 6 as a solid line. It spans almost three orders in magnitude, starting at about 19,000 J kg^{-1} s^{-1} at 0.3 AU and reaching about 19 J kg^{-1} s^{-1} at 20 AU. The partition between alphas and protons, $\varepsilon_\alpha/\varepsilon_p$, decreases from ~2.4 at 0.3 AU to ~1.3 at 20 AU, so more of the heating goes into the alpha particles and helps maintain their higher temperatures. The average required heating rate at 1 AU is about 2550 J kg^{-1} s^{-1}, with only 900 J kg^{-1} s^{-1} deposited to protons. *Smith et al.* [2001] tested a phenomenological theory for the turbulent heating of the solar wind. By fitting Voyager 2 observations, they gave an estimate for the proton heating rate at 1 AU to be 1600 J kg^{-1} s^{-1}, which is approximately 1.8 times the proton heating rate of ICMEs. As shown by equation (1), the proton heating rate ε_p is proportional to the temperature T_p. Given that the temperature is about 2 times higher in the solar wind than inside ICMEs, we consider the two estimates to be consistent.

3.2. Turbulence and Energy Dissipation Rate

[18] Examination of magnetic fluctuations within an ICME showed a power spectrum of the form $f^{-5/3}$ at spacecraft frequencies less than 0.5 Hz [*Leamon et al.*, 1998b]. Such an inertial range spectrum of the Kolmogoroff form indicates strong nonlinear couplings and quasi-steady spectral transfer. It is still not clear whether this property generally exists within ICMEs. We therefore consider two different theories that can be applied to the turbulence. One of them, Kolmogoroff phenomenology [*Kolmogoroff*, 1941], gives a simple expression for the inertial range omnidirectional spectrum of the turbulent energy (per unit mass per unit wave number)

$$E(k) = C_{ko}\varepsilon^{2/3}k^{-5/3} \quad (3)$$

in terms of the energy transfer rate ε and the wave number k. The numerical constant is $C_{ko} \simeq 1.6$. Kolmogoroff's theory describes incompressible hydrodynamic turbulence but is also applicable to magnetic fluctuations of the solar wind. *Kraichnan* [1965] modified the theory to include the effect of the magnetic field, which gave the MHD equivalent for the energy spectrum

$$E(k) = C_{kr}(\varepsilon v_A)^{1/2}k^{-3/2}, \quad (4)$$

where v_A is the Alfvén velocity. The above two formulations can be linked together by a phenomenological argument of the characteristic spectral transfer time [*Matthaeus and Zhou*, 1989]: the Kolmogoroff spectrum

corresponds to the limit of weak magnetic fields while the Kraichnan spectrum applies to the case of strong fields. The relation between the constants C_{kr} and C_{ko} is $C_{kr} = C_{ko}^{3/4}$ resulting from this argument, which gives $C_{kr} \simeq 1.42$.

[19] The trace of the observed power spectral matrix is related to the omnidirectional spectrum by (see equations (3.4.17) and (3.4.18) in the work of *Batchelor* [1953])

$$P(k) = P_{xx} + P_{yy} + P_{zz} = \int_{k}^{+\infty} \frac{E(k')}{k'} dk', \qquad (5)$$

where P_{xx}, P_{yy}, and P_{zz} are the power spectra of magnetic fluctuations in the x, y, and z components, respectively. Substituting equations (3) and (4) into the above equation, we can obtain the reduced Kolmogoroff and Kraichnan spectra $P(k)$ separately. Conversion of the power spectrum from the plasma-frame wave number k to the spacecraft-frame frequency f requires a correction for the Doppler shift, i.e., $k = \frac{2\pi f}{v \pm v_w(k)}$ for wave structures moving with velocity $v_w(k)$ superposed on the plasma speed v outward from (+) or toward (−) the Sun. Since the plasma flow speed is much larger than the characteristic speed of the fluctuations, this relation is simplified to $k = \frac{2\pi f}{v}$. Using this relation as well as $P(k)dk = P(f)df$ yields the reduced Kolmogoroff spectrum in terms of the spacecraft-frame frequency f

$$P(f) = \frac{3}{5} C_{ko} \varepsilon^{2/3} \left(\frac{2\pi}{v} \right)^{-2/3} f^{-5/3} \qquad (6)$$

and the Kraichnan counterpart

$$P(f) = \frac{2}{3} C_{kr} (\varepsilon v_A)^{1/2} \left(\frac{2\pi}{v} \right)^{-1/2} f^{-3/2}. \qquad (7)$$

Rearrangement of equations (6) and (7) gives the turbulence cascade rate

$$\varepsilon_{ko} = \left(\frac{5}{3C_{ko}} \right)^{3/2} \frac{2\pi}{v} f^{5/2} [P(f)]^{3/2} \qquad (8)$$

deduced from the Kolmogoroff spectrum and

$$\varepsilon_{kr} = \frac{9\pi}{2C_{ko}^2} \frac{1}{vv_A} f^3 [P(f)]^2 \qquad (9)$$

from the MHD equivalent. Note that $P(f)$ is the observed power spectral density in the inertial range. By inserting it into equations (8) and (9), two different specific dissipation rates can be obtained. Determination of the turbulence dissipation rate for the solar wind was performed in this way by *Coleman* [1968] and *Leamon et al.* [1999]. In addition, fitting the observed spectrum to a power law gives the spectral index. Comparison of the deduced heating rates with the required rates determines whether turbulence dissipation can explain the heating of ICMEs; together with the spectral index, this comparison will also determine which theory applies to the turbulence.

[20] We compute the power spectrum of magnetic fluctuations inside ICMEs from the magnetic field observations. We use 6 s averages of the magnetic field from the Helios missions and 1 s measurements from Ulysses. The Nyquist frequency for the Helios data is 0.083 Hz, which is usually below the proton gyrofrequency, so the dissipation range spectrum is not seen. In constructing the power spectrum, we first rotate the magnetic field observations into a field-aligned coordinate system following the approach of *Bieber et al.* [1996]. In this system, the z axis is aligned with the mean magnetic field and points away from the Sun, the x axis is in the plane defined by the mean field and the radial direction and also points away from the Sun, and the y axis completes the right-handed system. More specifically, the orthogonal mean field coordinates $(\hat{x}, \hat{y}, \hat{z})$ are the normalized $(\langle \mathbf{B} \rangle \times \hat{r} \times \langle \mathbf{B} \rangle, \langle \mathbf{B} \rangle \times \hat{r}, \langle \mathbf{B} \rangle)$, where $\langle \mathbf{B} \rangle$ is the mean field vector and $\hat{r}$ is the unit vector in the radial direction. We divide the ICME data into 1-hour intervals and the coordinates are set up using these 1-hour averages. In the new system, the B_z component is roughly the magnitude of the magnetic field and the components B_x and B_y are transverse fluctuations of the field. Trends in the B_x and B_y components are thereby automatically eliminated. Linear trends in the B_z component are subtracted after the coordinate system is established. Note that the coordinate system changes from one interval to another since the direction of the mean field $\langle \mathbf{B} \rangle$ changes. Intervals with more than 10% of the data missing are rejected; data gap filling is then performed for the rest of the intervals by a linear interpolation to ensure an equally spaced data record. The resulting intervals for each ICME are concatenated to form a series of data large enough to ensure sufficient frequency points in the inertial range of the power spectrum. The justification for this step is that the data are in the field-aligned coordinates with trends removed. Moreover, the inertial range power spectrum is associated with intermediate scale structures extending to the gyroradius of protons, while the dissipation range corresponds to even smaller structures. Presumably, these spectra are the same for different intervals of an ICME.

[21] The power spectrum of solar wind fluctuations is often estimated by the Blackman-Tukey technique [e.g., *Matthaeus and Goldstein*, 1982; *Leamon et al.*, 1998a]. The starting point of this method is that the spectral density is equal to the Fourier transform of the autocorrelation function. This method requires that the maximum lag used in calculating the autocorrelation function should be much smaller than the number of data samples to guarantee positive definiteness of the spectrum. In practice, a maximum lag is usually selected to be 10% of the length of the data for statistical validity. In the case of ICMEs, we frequently find that significant autocorrelation of the data exists even at much larger lags; the truncation of the function at 10% of the length thus gives a spurious spectrum. Here we use an improved periodogram estimator, the so-called Welch method (refer to the review by *Ghil et al.* [2002]). The data sequence of ICMEs is segmented into bins of the same length with adjacent bins half overlapping. The number of bins or the length of the bin is dictated by the tradeoff between the frequency resolution and estimated variance. A rule of thumb is to take the length M to be no larger than $N/5$ or $N/10$, where N is the number of data samples; in practice, we find that with $N/M = 8$ adequate statistical validity can be obtained. Each segment is then smoothed by the Hamming window before computing the
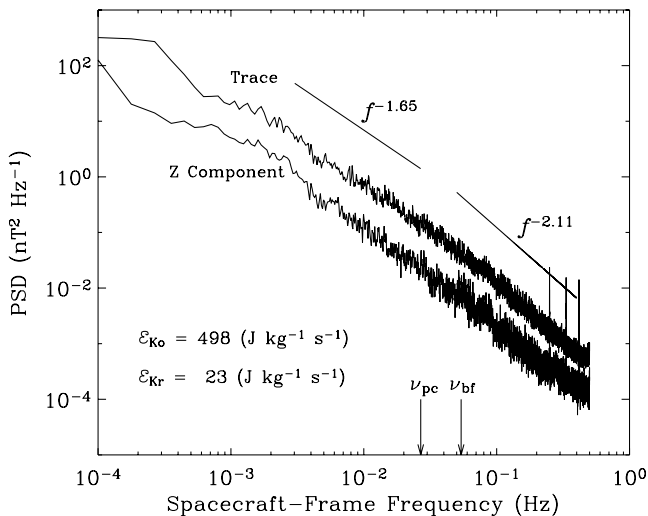
Figure 7. Power spectral density of magnetic fluctuations within an ICME observed by Ulysses at 3.25 AU. The inertial and dissipation ranges are shown by the power law fits with corresponding spectral indices. The proton cyclotron and spectral break frequencies are denoted by the arrows. Text in the lower left corner depicts the turbulence dissipation rates deduced from the Kolmogoroff and Kraichnan formulations, respectively.

transform, which helps attenuate the power leakage. The final spectrum is achieved by averaging the estimate over the bins in order to reduce the bias and variance. This procedure gives a robust spectrum which mostly lies above the 95% significance level in the frequency domain.

[22] Applying the above procedures to each component of the magnetic field, we obtain the power spectra P_{xx}, P_{yy}, and P_{zz}, respectively. In the field-aligned coordinates, P_{zz} is the power spectrum of fluctuations parallel to the field, i.e., $P_\parallel = P_{zz}$; the power of fluctuations perpendicular to the field is $P_\perp = P_{xx} + P_{yy}$ as discussed above. Figure 7 gives a typical ICME power spectrum calculated from 1 s magnetic field measurements by Ulysses at 3.25 AU on days 156–158.6 of 1991 from the list of *Liu et al.* [2005]. As required by the spectral estimator, data segmentation is implemented, and a frequency resolution of about 10^{-4} Hz is acquired. The trace of the power spectral matrix, i.e., $P = P_{xx} + P_{yy} + P_{zz}$, is shown in the figure as well as the z component P_{zz}. The power spectra show a slight but discernable steepening at high frequencies, indicative of the onset of magnetic dissipation. We fit the trace of the spectral matrix with a power law in the inertial and dissipation ranges separately; points close to the break frequency are omitted. The fit results are displayed in the plot. The spectral index in the inertial range is about 1.65 ± 0.02, in good agreement with the Kolmogoroff prediction of 5/3. The dissipation range spectrum has a slightly steeper form with an index of about 2.11 ± 0.01, smaller than the solar wind average level of 3.04 [*Leamon et al.*, 1998a]. Accordingly, the spectral cascade within ICMEs may tend to be low. The intersection of the two power laws enables us to compute the frequency at which the spectral break occurs. The resulting break frequency, ν_{bf}, is about 0.054 Hz, comparable to, but

larger than, the proton gyrofrequency $\nu_{pc} = 0.027$ Hz. The dissipation range of the spectrum is hence associated with the fluctuations with spatial scales smaller than the gyroradius of protons, which may indicate the presence of proton cyclotron damping. The energy cascade rate calculated from equation (8) is about 498 J kg^{-1} s^{-1}, much larger than the Kraichnan prediction of 23 J kg^{-1} s^{-1} from equation (9). In computing the dissipation rate, the power law fit of the inertial range $P(f)$ shown in Figure 7 is scaled to velocity units and then inserted into the two equations separately, and a geometric mean (the same as the arithmetic mean in this case) is taken over 270 frequency points in the range of 0.003 Hz up to the gyrofrequency. As can be seen from Figure 6, the required heating rate at 3.3 AU is about 400 J kg^{-1} s^{-1}, consistent with the Kolmogoroff dissipation rate but not the Kraichnan counterpart. This result, as well as the inertial range index, favors the Kolmogoroff turbulence theory.

[23] Another interesting feature of the spectrum is that the turbulence is highly two-dimensional in geometry. The compressive component (i.e., the z component) is a small faction of the total power in the inertial range, but this faction grows a little larger in the dissipation range. Therefore most of the energy resides in wave vectors perpendicular to the mean magnetic field in either the inertial or dissipation ranges. The above results are consistent with the characteristics of magnetic fluctuations within an MC obtained by *Leamon et al.* [1998b].

[24] Repeating the same procedure for each ICME yields the inertial range spectral index and the turbulent dissipation rate as a function of heliocentric distance. In fitting the inertial range spectrum, typically 100–200 frequency points in the range 0.005–0.05 Hz are used for the Helios 6 s averages depending on the sample length; for the Ulysses 1 s measurements, we adopt the frequency range from 0.005 Hz to the proton gyrofrequency containing about 300 spectral estimates. The turbulence cascade rates determined from equations (8) and (9) are displayed in Figure 6 to make a comparison with the required heating rate. The data are binned as in Figure 5, with the bin size denoted by the horizontal bars. The error bars show the range of data distribution within each bin. The dissipation rate, deduced from either the Kolmogoroff or Kraichnan formulations, shows a clear decrease with distance. The rate predicted by the Kraichnan theory is 2 orders of magnitude lower than the Kolmogoroff prediction and it is well below the rate required by the temperature profile. The dissipation rate determined from the Kolmogoroff formulation is sufficient to explain the heating of the ICME plasma. *Leamon et al.* [1999] studied magnetic dissipation based on a model of kinetic Alfvén waves and found that about 58% of the total dissipated energy in the solar wind goes to the heating of protons. They suggested that the remaining energy goes into electron heating. The required heating rate given here does not include the energy for electron heating, but the turbulence cascade rate still appears to be adequate if electron heating is included. The Kolmogoroff dissipation rate shows a large variation close to 1 AU, so a rigorous comparison with the solar wind counterpart is not available.

[25] The derived inertial-range spectral index q is shown in Figure 8, represented by the averages within the same
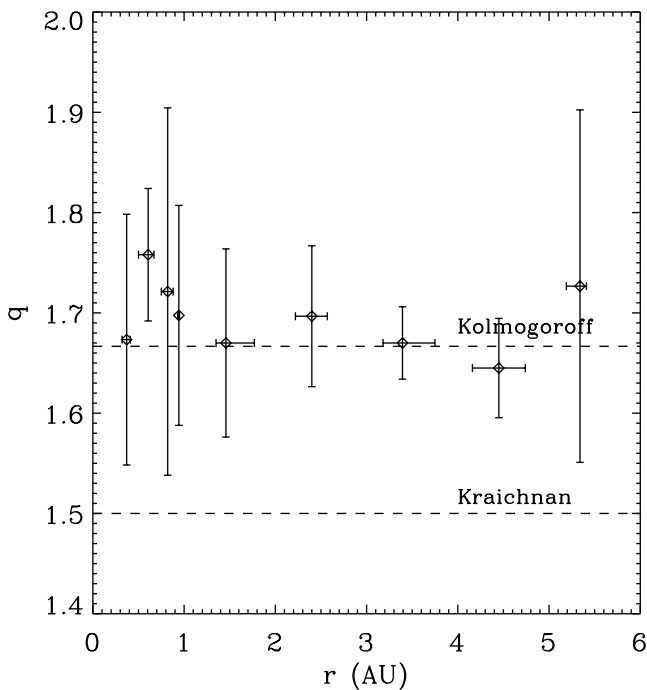
Figure 8. Inertial-range spectral indices as a function of heliocentric distance. The horizontal bars show the same bins as in Figure 6 and the error bars indicate the standard deviation of the data inside the bins. The Kolmogoroff index 5/3 and the Kraichnan level 3/2 are marked by the dashed lines.

solutions of the Vlasov dispersion equation or single fluid MHD equations. The lower bound of the temperature anisotropy is an MHD mode with $T_{\perp p} < T_{\parallel p}$, the so-called firehose instability, which has $S = -2$ and $\alpha = 1$ [*Parker*, 1958]. The upper bound is imposed by the cyclotron and mirror instabilities. By fitting the numerical solutions of the Vlasov dispersion equation, *Gary et al.* [1997] obtained $S = 0.64$ and $\alpha = 0.41$ for the cyclotron instability at the maximum growth rate $\gamma_m = 0.01 \, \Omega_p$ in the domain $0.1 \leq \beta_{\parallel p} \leq 10$, and $S = 0.87$, $\alpha = 0.56$ for the mirror instability at the same maximum growth rate over $5 \leq \beta_{\parallel p} \leq 50$. The enhanced magnetic fluctuations induced by the cyclotron instability are predominantly transverse, while the mirror instability leads to predominantly compressive fluctuations.

[28] Figure 9 illustrates the temperature ratio T_p/T_{ex} as a function of the temperature anisotropy and parallel plasma beta of protons. The procedure for creating this plot is the same as in Figure 4, but now it is applied to 100 s averages of the Wind observations which contain more than 640,000 spectra recorded between 1994 and 2004. Again, regions with denser measurements in the two-dimensional plane contain more cells, but no cell has fewer than 1000 data points. The data distribution is described by the black contours. As indicated by the contours, the typical solar wind has an anisotropy of ~ -0.35 and a parallel plasma beta of ~ 0.8. Therefore $T_{\perp p} \simeq 0.65 T_{\parallel p}$ on average at 1 AU. The threshold conditions of the instabilities are denoted by the lines of different styles in the figure. As can be seen, the majority of
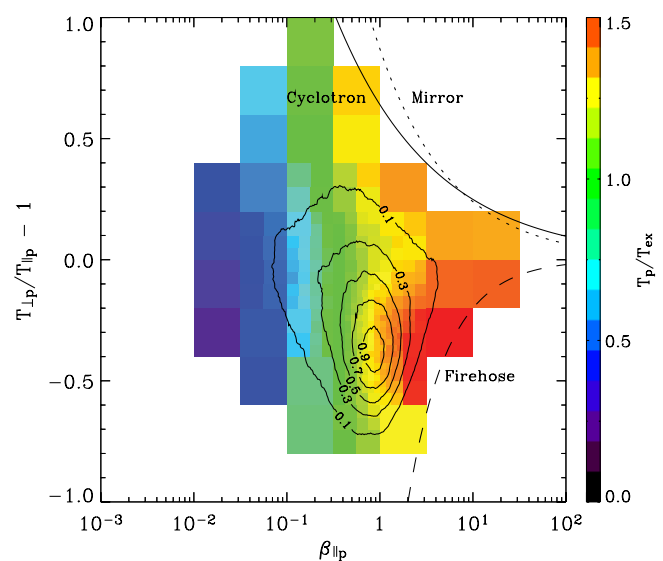
bins as in Figure 6. The standard deviations for the bins are plotted as error bars. The spectral index, with an average of 1.71, is generally larger than the Kraichnan prediction 3/2 but close to the Kolmogoroff index value of 5/3. Combined with the dissipation rate, this result verifies that the Kolmogoroff law, a crucial theorem for the inertial range turbulence, may also apply in the ICME plasma.

3.3. Source of Turbulence

[26] The Kolmogoroff form of the inertial range spectrum shows that magnetic fluctuations within ICMEs are essentially nonlinear. What is interesting here is that wave structures and large-scale flow gradients are not frequently seen within ICMEs. A question thus arises regarding what sources drive the turbulence.

[27] Enhanced magnetic fluctuations can derive from instabilities induced by temperature anisotropies. The free energy associated with the temperature anisotropy feeds rapidly growing magnetic fluctuations when the proton temperature ratio $T_{\perp p}/T_{\parallel p}$ exceeds certain threshold conditions. We thus examine these instabilities as possible mechanisms for generating magnetic turbulence in ICMEs. The thresholds for the onset of these instabilities can be written as [e.g., *Gary et al.*, 1994]

$$\frac{T_{\perp p}}{T_{\parallel p}} - 1 = \frac{S}{\beta_{\parallel p}^{\alpha}},$$

where the parallel plasma beta is defined as $\beta_{\parallel p} = \frac{n_p k_B T_{\parallel p}}{B^2/2\mu_0}$. Here S and α are free parameters which can be derived from

Figure 9. Survey of Wind measurements of the normalized proton temperature T_p/T_{ex} as a function of the temperature anisotropy and parallel plasma beta of protons. Bins are smaller in regions of higher-density measurements, but each bin contains at least 1000 spectra. The average values of T_p/T_{ex} within the bins are indicated by the color shading. Black contours show the density of observations at levels of [0.1, 0.3, 0.5, 0.7, 0.9]. Also shown are the thresholds for the firehose (dashed line), cyclotron (solid line), and mirror (dotted line) instabilities.

the data is constrained by the thresholds. This evidence confirms that the upper and lower bounds indeed exist for the temperature anisotropies. In this figure the color scale, given by the bar on the right, indicates the average values of T_p/T_{ex} within the intervals. The high temperature regions are near the thresholds. The enhanced magnetic fluctuations lead to significant plasma heating when the instabilities rise above the thresholds; the heating continues until the damping of instabilities pushes the temperature anisotropy back into the constrained regime. Also note that the proton temperature is more enlarged near the threshold for the firehose instability than near the upper bound. Since the firehose instability is a large-scale MHD mode, more energy may be transferred to the particles from the damping of this instability. These results provide the first consistent view of the plasma heating by instabilities driven by temperature anisotropies. As mentioned in section 2, $T_p/T_{ex} \leq 0.5$ is an indicator of ICME plasma. This figure clearly shows that the ICME region with low temperatures is characterized by $\beta_{\parallel p} \leq 0.1$ and located far away from the instability thresholds. A similar graph can also be constructed for the density ratio of n_α/n_p in the same plane (not shown here). Consistently, the high-density helium region roughly takes the same place in the plot. We conclude that instabilities due to temperature anisotropies do not play a role in the heating of ICMEs. Hence the source of the turbulence seen inside ICMEs in the inner heliosphere is still an open question.

[29] In the outer heliosphere (outside the ionization cavity), interactions between solar wind ions and interstellar neutrals are probably responsible for the solar wind heating. Since interstellar neutrals can freely penetrate plasmas, this interaction also occurs in ICMEs. Low-frequency MHD fluctuations can be generated by the damping of waves excited by pickup ions formed by the ionization of interstellar neutrals. In a steady state, this production of energy will be balanced by the dissipation rate. The heating rate associated with pickup ions can be estimated by [e.g., *Williams and Zank*, 1994]

$$\varepsilon_{pi} = \frac{f_D v_p v_A n_H}{n_p^0 \tau_{ion}^0}, \qquad (10)$$

where n_p^0 is the number density of protons at 1 AU taken from the fit in Figure 2, and τ_{ion}^0 is the neutral ionization time at 1 AU which is about 10^6 s. Here the Alfvén speed v_A is assumed to have a fixed value 50 km s^{-1}. We use the standard cold distribution for the density of interstellar neutrals [*Vasyliunas and Siscoe*, 1976]

$$n_H = n_H^\infty \exp(-\lambda/r), \qquad (11)$$

where n_H^∞ is the interstellar neutral density at the termination shock, and λ is the length scale of the ionization cavity taken to be 8 AU. The parameter f_D gives the faction of the available energy dissipated to the thermal core of protons. The value of f_D is ~0.05 based on fitting Voyager 2 observations assuming $n_H^\infty = 0.1$ cm^{-3} [*Smith et al.*, 2001].

[30] For completeness, we compare the above dissipation rate with the energy deposition calculated by *McNutt et al.* [1998] from the Boltzmann collision integrals. The charge exchange of interstellar neutrals with ions provides a source of both momentum and thermal energy. From their evaluation, the thermal energy can be expressed as

$$Q_t = 2k_B(T_H - T_p)\sigma(v^*)n_p n_H v^* + \frac{1}{2}m_p(v_H - v_p)^2\sigma(v_m^*)n_p n_H v_m^*, \qquad (12)$$

where T_H is the temperature of interstellar neutrals taken to be 10^4 K, and v_H is their speed assumed to be 20 km s^{-1}. The charge exchange cross section used in the above expression can be written as

$$\sigma(v) = (2.1 \times 10^{-7} - 9.2 \times 10^{-9} \ln v)^2 \text{ cm}^2 \qquad (13)$$

with speed v in units of cm s^{-1}. The two terms in equation (12) are associated with thermal energy exchange and momentum transfer between protons and neutrals, respectively. The characteristic speeds corresponding to the two exchanges can be approximated by

$$v^* = \sqrt{\frac{4}{\pi}\left(\frac{2k_B T_p}{m_p} + \frac{2k_B T_H}{m_p}\right) + (v_H - v_p)^2}, \qquad (14)$$

and

$$v_m^* = \sqrt{\frac{64}{9\pi}\left(\frac{2k_B T_p}{m_p} + \frac{2k_B T_H}{m_p}\right) + (v_H - v_p)^2}. \qquad (15)$$

The energy deposition rate is related to the thermal energy by

$$\varepsilon_{pi} = \frac{f_D Q_t}{n_p m_p}. \qquad (16)$$

Similarly, the energy partition factor f_D is also applied concerning the uncertainties.

[31] The energy deposition rates by pickup ions, estimated from equations (10) and (16) based on the fits in Figure 2, are plotted in Figure 6. The deposition rates determined from the two equations differ by a factor of 2, which indicates a rough consistency of the two approaches. The deposition rate shows a steady increase as distance and seems to match the required heating rate of ICMEs around 20 AU. Therefore the pickup ions should be the dominant source for the heating of the ICME plasma in the outer heliosphere. An increase in the ICME temperature might be expected since the deposition rate by pickup ions continues to grow with distance. One consequence is that the temperature criteria used in identifying ICMEs may not work beyond 20 AU. The identification of ICMEs is hence particularly difficult at large distances, which in turn makes the observational confirmation of the temperature increase hard to achieve.

4. Summary and Discussion

[32] We have presented a statistical study of the thermodynamic structure of ICMEs based on combined surveys of the ejecta between 0.3 and 20 AU from Helios 1 and 2,

Ulysses, and Voyager 1 and 2 data. The results are summarized and discussed as follows.

[33] We confirm the ICME expansion reported by *Liu et al.* [2005]. It is interesting to compare the observed expansion with theoretical predictions. In the flux-rope model of MCs proposed by *Kumar and Rust* [1996], the predicted expansion gives a radial width $W \sim r$, number density $n \sim r^{-3}$, magnetic field strength $B \sim r^{-2}$, and temperature $T \sim r^{-1}$. In this model the magnetic field configuration is essentially force-free within the flux rope, but the authors argued that a small angle of $4°$ between the current and the magnetic field can provide the necessary force to drive the expansion. Compared with the fits in Figures 1 and 2, the model yields a rather faster expansion. In good agreement with our results, the polytropic index obtained from the theoretical expansion is also $\gamma \sim 1.3$, so the ICME expansion is not adiabatic due to the local heating of the plasma.

[34] The ICME plasma is collision dominated. The expansion time of the plasma is generally comparable to or even larger than the Coulomb collision time. Restricted by the strong collisions, the differential speed between alpha particles and protons rapidly diminishes to below 10 km s^{-1} within ICMEs. However, the alpha particles have a higher temperature than protons with a typical temperature ratio $T_\alpha/T_p = 4–6$. The preferential heating of alphas, which overwhelms the energy loss to protons through Coulomb collisions, must be accounted for in any local heating mechanism.

[35] Magnetic dissipation is sufficient to explain the in situ heating of the ICME plasma. The inertial range spectrum of magnetic fluctuations within ICMEs frequently shows the Kolmogoroff form with spectral index 5/3, and the dissipation range, which begins at frequencies slightly larger than the proton cyclotron frequency, has a steeper slope. From the observed power spectrum in the inertial range, we deduce the energy dissipation rate and compare it with the required heating rate. We find that the Kolmogoroff law applies to the magnetic turbulence inside ICMEs and the dissipation rate determined from this formulation is adequate to produce the temperature profile.

[36] The occurrence of magnetic dissipation at frequencies comparable to the proton cyclotron frequency suggests resonant cyclotron damping of the fluctuations. The resonant cyclotron interaction is capable of accelerating and heating heavy ions preferentially [e.g., *Hollweg and Turner*, 1978]. *Isenberg and Hollweg* [1983] investigated the preferential heating and acceleration of solar wind alpha particles by this interaction with parallel-propagating ion cyclotron waves. *Hu and Habbal* [1999] extended this study by including the dispersive effect imposed by the alpha particles. Both of the studies show that the alpha particles can be preferentially heated by the cyclotron interaction to more than 4 times the proton temperature. The energy for this interaction was assumed to come from a nonlinear cascade of low-frequency Alfvén waves. However, Alfvén waves are seldom seen inside ICMEs and the ejecta show a relative lack of sources to drive the turbulence. We investigated the sources for the turbulence, particularly the instabilities driven by temperature anisotropies and energy deposition by pickup ions. The ICME plasma is not near the instability thresholds, so the

instabilities may not contribute to the turbulence generation. A rough estimate shows that the free energy associated with pickup ions is the dominant source for the ICME heating beyond 20 AU.

[37] Some other results should also be noted, although they are not of particular relevance to the purpose of this work. In the collisionless regime of the solar wind plasma with extremely high temperature and low helium abundance, the alpha particles and protons approach thermal equilibrium while they have a large relative drift (see Figure 4). The free energy associated with the differential streaming apparently does not feed the heating of this plasma; resonant cyclotron damping also seems unable to produce the high temperatures since it will preferentially heat the alpha particles and thus make them substantially hotter than protons. This plasma heating is not understood. Another interesting outcome is that temperature anisotropies of the solar wind are constrained by the threshold conditions for the firehose, mirror, and cyclotron instabilities (refer to Figure 9). Significant plasma heating occurs when the instabilities rise above the thresholds.

Appendix A: Collisions and Transport in an Expanding Plasma

[38] Consider a parcel of ICME plasma with volume V moving away from the Sun with a constant velocity v. The plasma expands in the solar wind and is characterized by a large temperature difference between the interacting alpha particles and protons. The effect of electrons can be ignored in the Coulomb energy transfer between different species of particles since their mass is very small. We start with the first law of thermodynamics for alpha particles

$$dU_\alpha = dQ_\alpha - P_\alpha dV, \tag{A1}$$

where dU_α is the change in the thermal energy of alphas, dQ_α is the heat added to them, and P_α is the alpha pressure. The internal energy can be expressed as

$$dU_\alpha = \frac{3}{2} N_\alpha k_B dT_\alpha, \tag{A2}$$

where N_α is the total number of alphas in the volume and k_B is the Boltzmann constant. In the presence of strong Coulomb collisions the quantity dQ_α includes heat transfer with protons and the energy from other sources. We treat the Coulomb energy exchange separately.

[39] To do so, we first consider an isolated plasma containing protons and alpha particles. If the plasma components have a large temperature difference but a small relative drift, the thermal equilibration via Coulomb collisions is described by

$$\left.\frac{dT_\alpha}{dt}\right|_c = \frac{T_p - T_\alpha}{\tau_{\alpha p}}. \tag{A3}$$

The Coulomb collision timescale $\tau_{\alpha p}$ can be written as

$$\tau_{\alpha p} = \frac{m_p + m_\alpha}{2 m_\alpha \nu_{\alpha p} \psi_{p\alpha}}, \tag{A4}$$

where m_p and m_α are the masses of protons and alphas, respectively. By assuming Maxwellian velocity distributions for the ion species, the momentum transfer frequency $\nu_{\alpha p}$ [*Burgers*, 1969] is given by

$$\nu_{\alpha p} = \frac{16\pi^{1/2}}{3} \frac{n_p m_p}{m_p + m_\alpha} \left(\frac{2k_B T_r}{m_r}\right)^{-3/2} \frac{e_p^2 e_\alpha^2}{m_r^2} \ln\Lambda, \quad (A5)$$

where e_p and e_α are the charges of protons and alphas, respectively. All units in the expressions are cgs except where noted. The reduced mass and temperature are defined by

$$m_r = \frac{m_p m_\alpha}{m_p + m_\alpha}, T_r = \frac{m_p T_\alpha + m_\alpha T_p}{m_p + m_\alpha}. \quad (A6)$$

The Coulomb logarithm [*Spitzer*, 1962] can be written for the ICME plasma as

$$\ln\Lambda \simeq 8.51 + 1.5\ln T_p - 0.5\ln n_p, \quad (A7)$$

by taking its radial dependence into account. The correction factor $\psi_{p\alpha}$ for the relative drift in equation (A4) is given by [cf. *Burgers*, 1969; *Schunk*, 1977]

$$\psi_{p\alpha} = \exp\left(-\frac{v_{\alpha p}^2}{v_t^2}\right), \quad (A8)$$

where $v_{\alpha p}$ is the differential speed between alphas and protons and v_t is the effective thermal speed defined as

$$v_t = \left(\frac{2k_B T_r}{m_r}\right)^{1/2}. \quad (A9)$$

Evidently, $\psi_{p\alpha} = 1$ in the limit of very small drifts ($v_{\alpha p} \ll v_t$), so it has a negligible effect in the case of ICMEs but may be significant for the solar wind.

[40] For the original problem, we write the heat dQ_α as

$$dQ_\alpha = \left(\frac{3}{2} N_\alpha k_B dT_\alpha\right)\bigg|_c + N_\alpha m_\alpha \varepsilon_\alpha dt, \quad (A10)$$

where the first term is the energy exchange through Coulomb collisions with protons and the second term is heat input from unknown sources. The quantity ε_α represents the specific heating rate of alphas with units J kg^{-1} s^{-1}. Combining equations (A2), (A3), and (A10), we can reduce equation (A1) to

$$\frac{dT_\alpha}{dt} = \frac{T_p - T_\alpha}{\tau_{\alpha p}} + \frac{2m_\alpha \varepsilon_\alpha}{3k_B} - \frac{2T_\alpha}{3V}\frac{dV}{dt}, \quad (A11)$$

where the ideal gas law $P_\alpha V = N_\alpha k_B T_\alpha$ is invoked. Conservation of the number of particles yields $\frac{dn_\alpha}{n_\alpha} = -\frac{dV}{V}$. We can then eliminate the volume V from the above equation, arriving at

$$\frac{dT_\alpha}{dr} = \frac{T_p - T_\alpha}{v\tau_{\alpha p}} - \frac{2T_\alpha}{3v\tau_e} + \frac{2m_\alpha \varepsilon_\alpha}{3k_B v}. \quad (A12)$$

Note that $dr = vdt$ is adopted for a purely radial outflow. We define τ_e as the expansion time of the plasma, which is expressed in the form

$$\tau_e = -\left(v\frac{d}{dr}\ln n_\alpha\right)^{-1} = -\left(v\frac{d}{dr}\ln n_p\right)^{-1}. \quad (A13)$$

For simplicity we assume that alphas and protons have the same bulk speed in the above equation. In observations their relative drift inside ICMEs quickly approaches zero due to strong Coulomb collisions. Any free energy associated with the drift can be included in the heating rate, ε_α.

[41] Note that the adiabatic cooling due to the expansion is described by the second term on the right-hand side of equation (A12). The adiabatic temperature profile $T_\alpha \propto r^{-4/3}$ can be recovered for the steady state with $n_\alpha \propto r^{-2}$ by omitting the first and third terms. Any expansion faster than r^{-2}, which will result in a faster temperature decrease without heating sources, can also be described by this equation. Whether the plasma is collision-dominated is determined by the magnitude of the ratio of $\tau_e/\tau_{\alpha p}$. Since ICMEs are characterized by very low temperatures but comparable densities with the solar wind, theoretically Coulomb collisions should be important in the transport equation, which can be readily seen from equations (A4), (A12), and (A13).

[42] Similarly, we can obtain the temperature equation for protons. It has the form

$$\frac{dT_p}{dr} = \frac{T_\alpha - T_p}{v\tau_{p\alpha}} - \frac{2T_p}{3v\tau_e} + \frac{2m_p\varepsilon_p}{3k_B v}, \quad (A14)$$

where ε_p is the corresponding specific rate of energy deposition to the protons. Note that in the above equation $\tau_{p\alpha}$ is related to $\tau_{\alpha p}$ by $\frac{\tau_{\alpha p}}{\tau_{p\alpha}} = \frac{n_\alpha}{n_p}$ (refer to equations (A4) and (A5)), which depends on what particles are treated as test particles. Here we use $\tau_{\alpha p}$ as an indicator for the Coulomb collision time, following the approach found in most of the literature [e.g., *Neugebauer*, 1976; *Marsch et al.*, 1982; *Neugebauer et al.*, 1996].

References

Batchelor, G. K. (Ed.) (1953), *The Theory of Homogeneous Turbulence*, Cambridge Univ. Press, New York.

Bieber, J. W., W. Wanner, and W. H. Matthaeus (1996), Dominant two-dimensional solar wind turbulence with implications for cosmic ray transport, *J. Geophys. Res.*, *101*, 2511.

Bothmer, V., and R. Schwenn (1998), The structure and origin of magnetic clouds in the solar wind, *Ann. Geophys.*, *16*, 1.

Burgers, J. M. (Ed.) (1969), *Flow Equations for Composite Gases*, Elsevier, New York.

Burlaga, L. F. (1988), Magnetic clouds and force-free fields with constant alpha, *J. Geophys. Res.*, *93*, 7217.

Cargill, P. J., D. S. Spicer, and S. T. Zalesak (1997), Magnetohydrodynamic simulations of Alfvénic pulse propagation in solar magnetic flux tubes: Two-dimensional slab geometries, *Astrophys. J.*, *488*, 854.

Coleman, P. J., Jr. (1968), Turbulence, viscosity, and dissipation in the solar-wind plasma, *Astrophys. J.*, *153*, 371.

Feldman, W. C., J. R. Asbridge, and S. J. Bame (1974), The solar wind He^{2+} to H$^+$ temperature ratio, *J. Geophys. Res.*, *79*, 2319.

Gary, S. P., M. E. McKean, D. Winske, B. J. Anderson, R. E. Denton, and S. A. Fuselier (1994), The proton cyclotron instability and the anisotropy/β inverse correlation, *J. Geophys. Res.*, *99*, 5903.

Gary, S. P., J. Wang, D. Winske, and S. A. Fuselier (1997), Proton temperature anisotropy upper bound, *J. Geophys. Res.*, *102*, 27,159.

Ghil, M., et al. (2002), Advanced spectral methods for climatic time series, *Rev. Geophys.*, *40*(1), 1003, doi:10.1029/2000RG000092.

Goldstein, M. L., D. A. Roberts, and W. H. Matthaeus (1995), Magnetohydrodynamic turbulence in the solar wind, *Annu. Rev. Astron. Astrophys.*, *33*, 283.

Hollweg, J. V., and J. M. Turner (1978), Acceleration of solar wind He^{++}: 3. Effects of resonant and nonresonant interactions with transverse waves, *J. Geophys. Res.*, *83*, 97.

Hu, Y.-Q., and S. R. Habbal (1999), Resonant acceleration and heating of solar wind ions by dispersive ion cyclotron waves, *J. Geophys. Res.*, *104*, 17,045.

Isenberg, P. A., and J. V. Hollweg (1983), On the preferential acceleration and heating of solar wind heavy ions, *J. Geophys. Res.*, *88*, 3923.

Kolmogoroff, A. N. (1941), Dissipation of energy in the locally isotropic turbulence, *C. R. Acad. Sci. URSS*, *32*, 16.

Kraichnan, R. H. (1965), Inertial range of hydromagnetic turbulence, *Phys. Fluids*, *8*, 1385.

Kumar, A., and D. M. Rust (1996), Interplanetary magnetic clouds, helicity conservation, and current-core flux ropes, *J. Geophys. Res.*, *101*, 15,667.

Leamon, R. J., C. W. Smith, N. F. Ness, W. H. Matthaeus, and H. K. Wong (1998a), Observational constraints on the dynamics of the interplanetary magnetic field dissipation range, *J. Geophys. Res.*, *103*, 4775.

Leamon, R. J., C. W. Smith, and N. F. Ness (1998b), Characteristics of magnetic fluctuations within coronal mass ejections: The January 1997 event, *Geophys. Res. Lett.*, *25*, 2505.

Leamon, R. J., C. W. Smith, N. F. Ness, and H. K. Wong (1999), Dissipation range dynamics: Kinetic Alfvén waves and the importance of β_e, *J. Geophys. Res.*, *104*, 22,331.

Liu, Y., J. D. Richardson, and J. W. Belcher (2005), A statistical study of the properties of interplanetary coronal mass ejections from 0.3 to 5.4 AU, *Plan. Space Sci*, *53*, 3.

Lopez, R. E. (1987), Solar cycle invariance in solar wind proton temperature relationships, *J. Geophys. Res.*, *92*, 11,189.

Manchester, W. B., T. I. Gombosi, I. Roussev, A. Ridley, D. L. De Zeeuw, I. V. Sokolov, K. G. Powell, and G. Tóth (2004), Modeling a space weather event from the Sun to the Earth: CME generation and interplanetary propagation, *J. Geophys. Res.*, *109*, A02107, doi:10.1029/2003JA010150.

Marsch, E., K.-H. Mühlhäuser, H. Rosenbauer, R. Schwenn, and F. M. Neubauer (1982), Solar wind helium ions: Observations of the Helios solar probes between 0.3 and 1 AU, *J. Geophys. Res.*, *87*, 35.

Matthaeus, W. H., and M. L. Goldstein (1982), Measurements of the rugged invariance of Magnetohydrodynamic turbulence in the solar wind, *J. Geophys. Res.*, *87*, 6011.

Matthaeus, W. H., and Y. Zhou (1989), Extended inertial range phenomenology of magnetohydrodynamic turbulence, *Phys. Fluids B*, *1*, 1929.

Matthaeus, W. H., G. P. Zank, C. W. Smith, and S. Oughton (1999), Turbulence, spatial transport, and heating of the solar wind, *Phys. Rev. Lett.*, *82*, 3444.

McNutt, R. L., Jr., J. Lyon, and C. C. Goodrich (1998), Simulations of the heliosphere: Model, *J. Geophys. Res.*, *103*, 1905.

Neugebauer, M. (1976), The role of Coulomb collisions in limiting differential flow and temperature differences in the solar wind, *J. Geophys. Res.*, *81*, 78.

Neugebauer, M., and R. Goldstein (1997), Particle and field signatures of coronal mass ejections in the solar wind, in *Coronal Mass Ejections*, *Geophys. Monogr. Ser.*, vol. 99, edited by N. Crooker, J. A. Joselyn, and J. Feynman, pp. 245, AGU, Washington, D. C.

Neugebauer, M., B. E. Goldstein, E. J. Smith, and W. C. Feldman (1996), Ulysses observations of differential alpha-proton streaming in the solar wind, *J. Geophys. Res.*, *101*, 17,047.

Odstrcil, D., J. A. Linker, R. Lionello, Z. Mikic, P. Riley, V. J. Pizzo, and J. G. Luhmann (2002), Merging of coronal and heliospheric numerical two-dimensional MHD models, *J. Geophys. Res.*, *107*(A12), 1493, doi:10.1029/2002JA009334.

Parker, E. N. (1958), Dynamical instability in an anisotropic ionized gas of low density, *Phys. Rev.*, *109*, 1874.

Reisenfeld, D. B., S. P. Gary, J. T. Gosling, J. T. Steinberg, D. J. McComas, B. E. Goldstein, and M. Neugebauer (2001), Helium energetics in the high-latitude solar wind: Ulysses observations, *J. Geophys. Res.*, *106*, 5693.

Richardson, I. G., and H. V. Cane (1993), Signatures of shock drivers in the solar wind and their dependence on the solar source location, *J. Geophys. Res.*, *98*, 15,295.

Riley, P., J. A. Linker, Z. Mikic, D. Odstrcil, T. H. Zurbuchen, D. Lario, and R. P. Lepping (2003), Using an MHD simulation to interpret the global context of a coronal mass ejection observed by two spacecraft, *J. Geophys. Res.*, *108*(A7), 1272, doi:10.1029/2002JA009760.

Schunk, R. W. (1977), Mathematical structure of transport equations for multispecies flows, *Rev. Geophys.*, *15*, 429.

Smith, C. W., W. H. Matthaeus, G. P. Zank, N. F. Ness, S. Oughton, and J. D. Richardson (2001), Heating of the low-latitude solar wind by dissipation of turbulent magnetic fluctuations, *J. Geophys. Res.*, *106*, 8253.

Spitzer, L., Jr., (Ed.) (1962), *Physics of Fully Ionized Gases*, 2nd ed., Interscience, New York.

Suess, S. T. (1988), Magnetic clouds and the pinch effect, *J. Geophys. Res.*, *93*, 5437.

Vasyliunas, V. M., and G. L. Siscoe (1976), On the flux and energy spectrum of interstellar ions in the solar system, *J. Geophys. Res.*, *81*, 1247.

Wang, C., and J. D. Richardson (2004), Interplanetary coronal mass ejections observed by Voyager 2 between 1 and 30 AU, *J. Geophys. Res.*, *109*, A06104, doi:10.1029/2004JA010379.

Williams, L. L., and G. P. Zank (1994), Effect of magnetic field geometry on the wave signatures of the pickup ions of interstellar neutrals, *J. Geophys. Res.*, *99*, 19,229.

————————

J. W. Belcher, J. C. Kasper, Y. Liu, and J. D. Richardson, Kavli Institute for Astrophysics and Space Research, Massachusetts Institute of Technology, Building 37-676a, Cambridge, MA 02139, USA. (liuxying@space.mit.edu)

H. A. Elliott, Space Science and Engineering, Southwest Research Institute, 6220 Culebra Road, San Antonio, TX 78228-0510, USA.